Enhanced Predictive Torque Control for Open End Winding Induction Motor Drive Without Weighting Factor Assignment

Ravi Eswar Kodumur Meesala, Venkata Praveen Kumar Kunisetti, and Vinay Kumar Thippiripati, *Member, IEEE*

***Abstract*—Nowadays, predictive torque control (PTC) is the most popular control technique in the field of electric drives. This PTC strategy is introduced for open end winding induction motor (OEWIM) drive in view of advantages. The conventional PTC offers a single-cost function where torque and stator flux control objectives are present. Since these control objectives are dissimilar, weighting factor designation to the respective control objective is essential. Weighting factor tuning by an empirical approach leads to a cumbersome control process. To overcome this tuning problem, this paper suggests a single control objective containing stator reference and predicted flux space vectors. This simplified proposed control scheme relieves PTC from weighting factor and facilitates combined torque and flux control. However, to control inverter switching frequency including torque and flux in a single cost function, weighting factors assignment and its proper tuning is indispensable. The proposed scheme is extended by replacing a single-cost function with separate multiobjectives and its optimization is achieved using a simple ranking analysis with limited prediction voltage vectors (VVs). This proposed feature permits PTC independent from weighting factors. Simulation and experimentation are performed on a dual inverter fed OEWIM drive. The achieved results are related with conventional PTC to verify the effectiveness of the proposed PTC.**

***Index Terms*—Open end winding induction motor drive (OEWIM), predictive torque controls (PTC), ranking analysis, and stator flux space vector control.**

I. Introduction

VOLTAGE source inverter (VSI) fed induction motor (IM) drive became much popular for industrial drive applications. Present research is to use multilevel inverters owing to the availability of greater number of VVs. It results in improved torque and flux regulation and accurate control of electric drive [1]. Various multilevel VSI topologies are documented in [2] and [3]. Apart from these, a dual inverter fed open end winding IM (OEWIM) configuration achieves salient status. The merits of the configuration are: simple, attaining multilevel inversion with a conventional two-level VSIs, absence of clamping diodes compared to a neutral point clamped topology, reduced number of dc voltage sources compared to a cascaded H-bridge inverter. The OEWIM drive's various applications are presented in [4]. The dynamic performance of a drive can be enhanced by employing several control techniques. The invention of field-oriented control technique in the year 1968 created remarkable development in the field of electric drive controlling [5]–[7]. In this technique, controlling is realized in a rotating reference frame. The necessity of PI current controllers, reference frame transformations, and rotor flux observer creates complex controlling. These demerits vanished with the introduction of the direct torque control technique in the year 1986. It uses hysteresis-based controllers (torque and flux) and provides direct torque and flux controlling in a stationary reference frame by selecting a suitable VV [8]. Its limitations are as follows: digital platform implementation demands high sampling frequency owing to the presence of nonlinear hysteresis controllers, poor torque and flux regulation, switching frequency relying on motor speed, and hysteresis bands. The mentioned limitations are addressed in [9]–[12].

Recently, model predictive control (MPC) technique is playing a prominent role in the area of electrical engineering [13]. It can be worked for both power converter and electric drive applications [14]–[17]. In [18], a detailed review is carried out on a predictive control scheme for power electronics. MPC has two divisions: continuous set MPC and finite set MPC (FS-MPC). The application of FS-MPC technique in the field of motor control is classified as predictive current control and predictive torque control (FS-PTC). Recently, FS-PTC has gained much importance owing to the following merits: simple and straightforward regulation by inclusion of control parameters into the cost function, good dynamic control, intuitive nature, lack of hysteresis controllers, and heuristic lookup tables. PTC performs a control action on the basis of cost function depreciation. This implies that cost function formulation plays a vital role in control performance. Cost function is formulated with a number of control objectives based on requirements [19]–[21]. The dissimilarities in control objectives and to provide relative importance among them demand weighting factor assignment to the respective objective. Therefore, weighting factor consideration in a cost function has a direct influence on the control performance. This has become the main problem

Manuscript received September 27, 2017; revised January 7, 2018; accepted February 26, 2018. Date of publication March 6, 2018; date of current version November 19, 2018. Recommended for publication by Associate Editor R. Kennel. *(Corresponding author: Vinay Kumar Thippiripati.)*

The authors are with the Department of Electrical Engineering, National Institute of Technology, Warangal 506004, India (e-mail: nit.ravieswar@gmail.com; kvpraveenkumar15@gmail.com; tvinay.nitw@gmail.com).

Color versions of one or more of the figures in this paper are available online at http://ieeexplore.ieee.org.

Digital Object Identifier 10.1109/TPEL.2018.2812760

in this control area and leads to many research works these days.

In [21], Cortes *et al*. suggested empirical procedures to solve the weighting factor selection problem. However, this results in weighting factor approximation but not optimal selection. In [22]–[25], the predictive control of an IM is performed while deciding the weights empirically. In [26], an analytical method is carried out to attain an optimal weighting factor for a three-phase VSI fed IM. In [27], PTC of an IM fed by an indirect matrix converter is performed, where an optimized weighting factor is considered for a control process. However, [26], [27] are examined with only flux and torque control objectives. It implicates complex control and system parameter reliant. In [28], a multiobjective genetic algorithm supported approach is applied for weights optimization, which demands a lot of search procedure prior to control. In [29], PTC of an IM fed by a two-level VSI is conducted while eliminating a flux weighting factor. Here [29], ranking analysis is performed for all the possible prediction VVs by considering torque and flux control objectives separately. However, its implementation without limiting number of prediction VVs makes the control process complex. In [30] and [31], multidecision criteria based TOPSIS and VIKOR methods are presented for IM drive control. However, in this process, weighting factor coefficients are not completely eliminated. In [32], predictive control of a matrix converter for the application of VAR compensation is performed, where the optimal weight is determined in every sample interval by autotuning of the weighting factor. In [33], fuzzy-based PTC is performed for an IM drive to alleviate weighting factors tuning. However, priority coefficient tuning is required which are assigned to membership function. In [34] and [35], PTC for OEWIM drive is introduced, where empirical weighting factors are assigned to the respective control objective in cost function. The tuning of these weighting factors becomes difficult and time overwhelming with the increase in the number of objectives.

This paper introduces a modified PTC for the OEWIM drive. The requirement of a weighting factor for torque and stator flux control objectives can be eliminated. Cost function is modified with a single control objective having stator reference and predicted flux space vectors. This feature enables combined torque and stator flux control with a single objective; thereby, eliminating the burden of flux weighting factor tuning. To limit the switching frequency of the OEWIM drive, an additional control objective needs to be added to the existing ones in the cost function. Owing to the dissimilar objectives in the single cost function, it demands weighting factor assignment. The proposed scheme is further extended to alleviate this problem by a simple ranking analysis with limited prediction VVs. This complete modified feature improves the control response of the OEWIM drive and limits switching frequency.

This paper is arranged as follows. Section II states the OEWIM configuration and mathematical modeling. Section III is related to the basic PTC in detail. Section IV presents the proposed PTC scheme and its extension for the OEWIM drive. Section V is related to the simulation and hardware validation of the proposed PTC scheme for the OEWIM drive. Finally, in Section VI, conclusion is derived which is satisfactory.

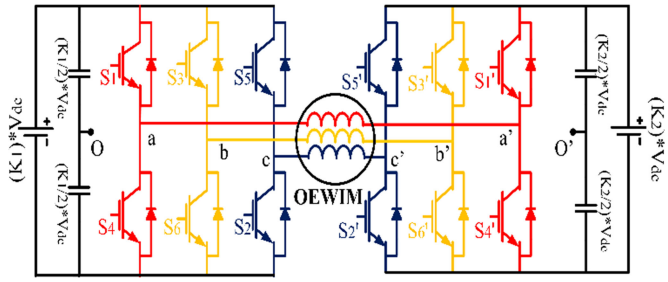

Fig. 1. OEWIM fed by dual inverter.

II. OEWIM Mathematical Modeling

The dual inverter (VSI-1 and VSI-2) fed OEWIM configuration is represented in Fig. 1. To attain a four-level inversion [4], the dual inverter dc-link voltages are maintained in the ratio of 2:1. Therefore, VSI-1 and VSI-2 dc-link voltages are set to $2V_{\rm dc}/3$ and $V_{\rm dc}/3$, respectively. Pole voltages of a dual inverter are stated by (1) and (2). The addition of pole voltage difference stated in (3) results in a nonzero term, named as zero sequence voltage. It is represented as (4). By substituting (4) in (5), phase voltages are represented in terms of pole voltages stated by (6):

$$\begin{pmatrix} V_{ao} \\ V_{bo} \\ V_{co} \end{pmatrix} = \begin{pmatrix} S_a \\ S_b \\ S_c \end{pmatrix} * (K_1 V_{\rm dc}) \tag{1}$$

$$\begin{pmatrix} V_{a'o'} \\ V_{b'o'} \\ V_{c'o'} \end{pmatrix} = \begin{pmatrix} S_{a'} \\ S_{b'} \\ S_{c'} \end{pmatrix} * (K_2 V_{\rm dc}) \tag{2}$$

where K_1 and K_2 are constants which are assigned as $K_1 = 2/3$ and $K_2 = 1/3$

$$\begin{pmatrix} \delta V_{aa'} \\ \delta V_{bb'} \\ \delta V_{cc'} \end{pmatrix} = \begin{pmatrix} V_{ao} - V_{a'o'} \\ V_{bo} - V_{b'o'} \\ V_{co} - V_{c'o'} \end{pmatrix} \tag{3}$$

$$V_z = \frac{(\delta V_{aa'} + \delta V_{bb'} + \delta V_{cc'})}{3} \tag{4}$$

$$\begin{pmatrix} V_{aa'} \\ V_{bb'} \\ V_{cc'} \end{pmatrix} = \begin{pmatrix} \delta V_{aa'} \\ \delta V_{bb'} \\ \delta V_{cc'} \end{pmatrix} - \begin{pmatrix} V_Z \\ V_Z \\ V_Z \end{pmatrix} \tag{5}$$

$$\begin{pmatrix} V_{aa'} \\ V_{bb'} \\ V_{cc'} \end{pmatrix} = \begin{pmatrix} 2/3 & -1/3 & -1/3 \\ -1/3 & 2/3 & -1/3 \\ -1/3 & -1/3 & 2/3 \end{pmatrix} * \begin{pmatrix} \delta V_{aa'} \\ \delta V_{bb'} \\ \delta V_{cc'} \end{pmatrix}. \tag{6}$$

OEWIM is modeled in a stationary frame of reference [36]. Its mathematical equations of voltage and flux linkage space vectors are stated by (7)–(9). Equation (10) states the generated motor torque and motor-load torque equation is given as (11)

$$\boldsymbol{V_s} = R_s \boldsymbol{i_s} + p\boldsymbol{\lambda_s} \tag{7}$$

$$0 = R_r \boldsymbol{i_r} + p\boldsymbol{\lambda_r} - j\omega_r \boldsymbol{\lambda_r} \tag{8}$$

$$\boldsymbol{\lambda_s} = L_s \boldsymbol{i_s} + L_m \boldsymbol{i_r}, \text{and } \boldsymbol{\lambda_r} = L_r \boldsymbol{i_r} + L_m \boldsymbol{i_s} \tag{9}$$

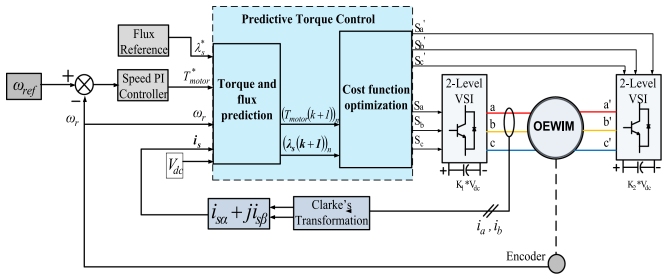

Fig. 2. Basic PTC for OEWIM drive.

$$T_{\text{motor}} = \frac{3}{2}\frac{P}{2}\left(\text{imag}\left(\bar{\boldsymbol{\lambda}}_{\boldsymbol{s}} \otimes \boldsymbol{i}_{\boldsymbol{s}}\right)\right) \tag{10}$$

$$T_{\text{motor}} - T_{\text{load}} = J\frac{d\omega_m}{dt}. \tag{11}$$

Here subscript "*s*" and "*r*" denote stator and rotor terms, respectively, and *P* represents number of poles in a machine. Motor mechanical and electrical speeds are represented by terms ω_m and ω_r, respectively. Stator current ($\boldsymbol{i}_s$) and flux linkage ($\boldsymbol{\lambda}_s$) space vectors are considered as state variables. Thus, state-space representation of IM model is stated by (12) and (13). The discrete form of (12) and (13) is utilized in the PTC algorithm

$$\frac{di_s}{dt} = C_1\left(C_2\boldsymbol{\lambda}_{\boldsymbol{s}} - C_3 i_s + K_r\left(\boldsymbol{V}_{\boldsymbol{s}} - Ci_s - j\omega_r\boldsymbol{\lambda}_{\boldsymbol{s}}\right) + \frac{j\omega_r i_s}{C_1}\right) \tag{12}$$

$$\frac{d\boldsymbol{\lambda}_{\boldsymbol{s}}}{dt} = \left(\boldsymbol{V}_{\boldsymbol{s}} - Ci_s\right) \tag{13}$$

where

$$\left.\begin{array}{l} C = R_s,\ C_1 = \frac{L_m}{L_s L_r - {L_m}^2},\ C_2 = \frac{R_r}{L_m},\ C_3 = \frac{L_s R_r}{L_m},\ p = \frac{d}{dt}, \\ K_r = \frac{L_r}{L_m},\ i_s = i_{s\alpha} + ji_{s\beta},\ \boldsymbol{\lambda}_{\boldsymbol{s}} = \lambda_{s\alpha} + j\lambda_{s\beta}, \\ \boldsymbol{V}_{\boldsymbol{s}} = V_{s\alpha} + jV_{s\beta} \end{array}\right\}. \tag{14}$$

III. Basic PTC

The required inputs for conventional PTC implementation are: motor speed (ω_r), stator current ($\boldsymbol{i}_s$), combined dc-link voltage (V_{dc}), reference torque (generated from speed PI controller), and reference flux magnitude (λ_s^*). Its operational block diagram is shown in Fig. 2. The main steps engaged in PTC are explained as follows.

A. Measurement and Estimation

In PTC of the IM drive, stator flux has to be estimated as the direct measurement is not possible. For this, forward Euler's method is used. The basic illustration of it is stated by (15). Here, the term v represents any state variable, k represents the present state, and T_s is the sample interval.

$$\frac{dv}{dt} = \frac{v\left(k+1\right) - v\left(k\right)}{T_s}. \tag{15}$$

The same is applied in (13) to estimate stator flux as follows:

$$\boldsymbol{\lambda}_s\left(\boldsymbol{k}\right) = \boldsymbol{\lambda}_s\left(\boldsymbol{k}-\boldsymbol{1}\right) + V_s T_s - CT_s i_s. \tag{16}$$

TABLE I
Effective Switching States and VV Realization

VSI-I	VSI-II	Space Vector	Realization	
(S_a,S_b,S_c)	(S'_a,S'_b,S'_c)	$\mathbf{V_s}$	$V_{s\alpha}$	$V_{s\beta}$
(0,0,0)	(0,0,0)	V_0	0	0
(1,0,0)	(1,0,0)	V_1	$V_{\text{dc}}(0.222)$	0
(1,1,0)	(1,1,0)	V_2	$V_{\text{dc}}(0.11)$	$(0.193)\,V_{\text{dc}}$
(0,1,0)	(0,1,0)	V_3	$V_{\text{dc}}(-0.11)$	$(0.193)\,V_{\text{dc}}$
(0,1,1)	(0,1,1)	V_4	$V_{\text{dc}}(-0.222)$	0
(0,0,1)	(0,0,1)	V_5	$V_{\text{dc}}(-0.11)$	$(-0.193)\,V_{\text{dc}}$
(1,0,1)	(1,0,1)	V_6	$V_{\text{dc}}(0.11)$	$(-0.193)\,V_{\text{dc}}$
(1,0,0)	(1,1,1)	V_7	$V_{\text{dc}}(0.444)$	0
(1,0,0)	(1,0,1)	V_8	$V_{\text{dc}}(0.33)$	$(0.193)\,V_{\text{dc}}$
(1,1,0)	(1,1,1)	V_9	$V_{\text{dc}}(0.222)$	$(0.385)\,V_{\text{dc}}$
(0,1,0)	(0,1,1)	V_{10}	0	$(0.385)\,V_{\text{dc}}$
(0,1,0)	(1,1,1)	V_{11}	$V_{\text{dc}}(-0.222)$	$(0.385)\,V_{\text{dc}}$
(0,1,0)	(1,1,0)	V_{12}	$V_{\text{dc}}(-0.33)$	$(0.193)\,V_{\text{dc}}$
(0,1,1)	(1,1,1)	V_{13}	$V_{\text{dc}}(-0.444)$	0
(0,0,1)	(1,0,1)	V_{14}	$V_{\text{dc}}(-0.33)$	$(-0.193)\,V_{\text{dc}}$
(0,0,1)	(1,1,1)	V_{15}	$V_{\text{dc}}(-0.222)$	$(-0.385)\,V_{\text{dc}}$
(0,0,1)	(0,1,1)	V_{16}	0	$(-0.385)\,V_{\text{dc}}$
(1,0,1)	(1,1,1)	V_{17}	$V_{\text{dc}}(0.222)$	$(-0.385)\,V_{\text{dc}}$
(1,0,0)	(1,1,0)	V_{18}	$V_{\text{dc}}(0.33)$	$(-0.193)\,V_{\text{dc}}$
(1,0,0)	(0,1,1)	V_{19}	$V_{\text{dc}}(0.667)$	0
(1,0,0)	(0,0,1)	V_{20}	$V_{\text{dc}}(0.55)$	$(0.193)\,V_{\text{dc}}$
(1,1,0)	(0,1,1)	V_{21}	$V_{\text{dc}}(0.44)$	$(0.385)\,V_{\text{dc}}$
(1,1,0)	(0,0,1)	V_{22}	$V_{\text{dc}}(0.33)$	$(0.577)\,V_{\text{dc}}$
(1,1,0)	(1,0,1)	V_{23}	$V_{\text{dc}}(0.11)$	$(0.577)\,V_{\text{dc}}$
(0,1,0)	(0,0,1)	V_{24}	$V_{\text{dc}}(-0.11)$	$(0.577)\,V_{\text{dc}}$
(0,1,0)	(1,0,1)	V_{25}	$V_{\text{dc}}(-0.33)$	$(0.577)\,V_{\text{dc}}$
(0,1,0)	(1,0,0)	V_{26}	$V_{\text{dc}}(-0.44)$	$(0.385)\,V_{\text{dc}}$
(0,1,1)	(1,0,1)	V_{27}	$V_{\text{dc}}(-0.55)$	$(0.193)\,V_{\text{dc}}$
(0,1,1)	(1,0,0)	V_{28}	$V_{\text{dc}}(-0.667)$	0
(0,1,1)	(1,1,0)	V_{29}	$V_{\text{dc}}(-0.55)$	$(-0.193)\,V_{\text{dc}}$
(0,0,1)	(1,0,0)	V_{30}	$V_{\text{dc}}(-0.44)$	$(-0.385)\,V_{\text{dc}}$
(0,0,1)	(1,1,0)	V_{31}	$V_{\text{dc}}(-0.33)$	$(-0.577)\,V_{\text{dc}}$
(0,0,1)	(0,1,0)	V_{32}	$V_{\text{dc}}(-0.11)$	$(-0.577)\,V_{\text{dc}}$
(1,0,1)	(1,1,0)	V_{33}	$V_{\text{dc}}(0.11)$	$(-0.577)\,V_{\text{dc}}$
(1,0,1)	(0,1,0)	V_{34}	$V_{\text{dc}}(0.33)$	$(-0.577)\,V_{\text{dc}}$
(1,0,1)	(0,1,1)	V_{35}	$V_{\text{dc}}(0.44)$	$(-0.385)\,V_{\text{dc}}$
(1,0,0)	(0,1,0)	V_{36}	$V_{\text{dc}}(0.55)$	$(-0.193)\,V_{\text{dc}}$

The machine stator currents (i_a, i_b, and i_c) can be sensed and subjected to Clarke's transformation. With this, resultant stator current space vector ($\boldsymbol{i}_s$) is obtained.

B. Prediction

With the available switching states of inverter configuration, prediction is done for stator current, flux, and torque of a machine. For a dual inverter fed OEWIM, there are "37" effective possible inverter switching states out of "64." The dual inverter voltage space vectors are stated by (17) and (18). From these, net voltage space vector is realized in (19) for a given machine as follows:

$$V_{s\boldsymbol{1}} = \left(\frac{2}{3}\right)\left(K_1 * V_{\text{dc}}\right)\left(S_a + S_b e^{j2\pi/3} + S_c e^{j4\pi/3}\right) \tag{17}$$

$$V_{s\boldsymbol{2}} = \left(\frac{2}{3}\right)\left(K_2 * V_{\text{dc}}\right)\left(S_a{}' + S_b{}' e^{j2\pi/3} + S_c{}' e^{j4\pi/3}\right) \tag{18}$$

$$V_{\boldsymbol{s}} = V_{\boldsymbol{s1}} - V_{\boldsymbol{s2}}. \tag{19}$$

Table I states "37" effective switching combinations and net voltage space vector (V_s) realization in a stationary reference frame. The voltage space vector (V_s) allocations are presented in

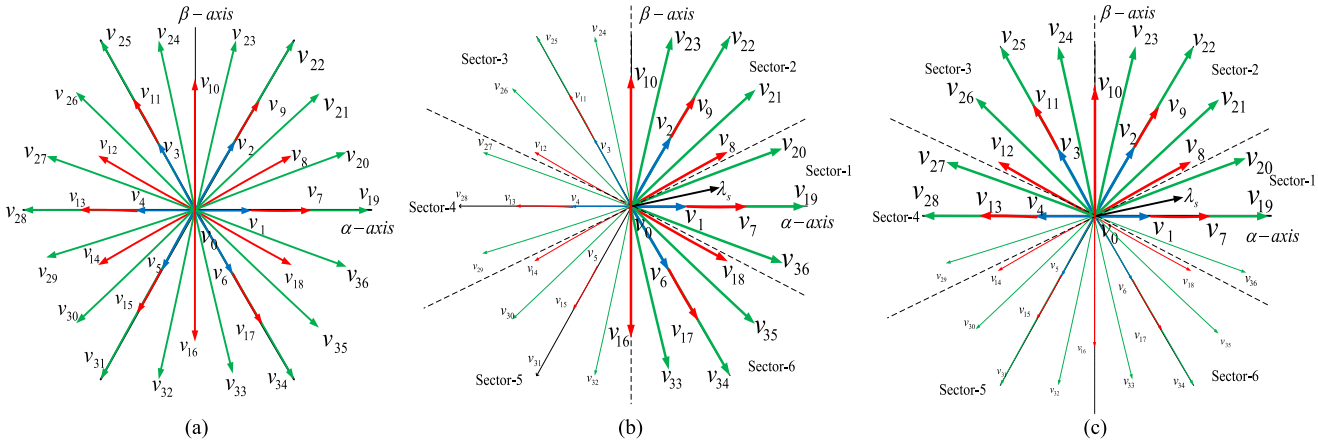

Fig. 3. (a) Complete voltage space vector allocations for dual inverter fed OEWIM. With the location of stator flux space vector in Sector 1, possible prediction VVs in dark color. (b) For $\Delta\lambda_s \geq 0$. (c) For $\Delta T \geq 0$.

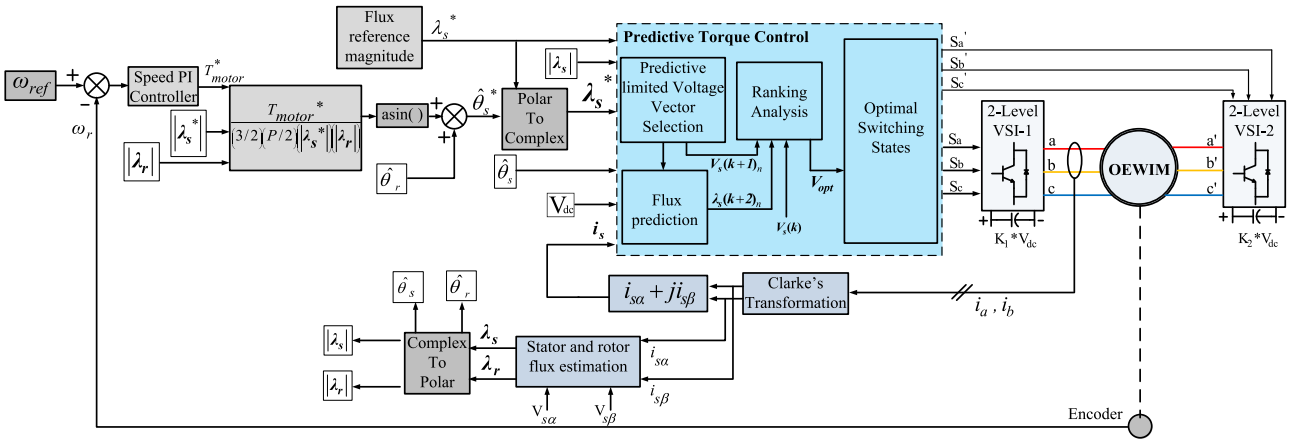

Fig. 4. Proposed PTC block diagram.

Fig. 3(a). From these, stator current, flux, and torque predictions for one step ahead $(k+1)$ are stated by the following:

$$\boldsymbol{\lambda}_s(\boldsymbol{k+1})_n = \boldsymbol{\lambda}_s(\boldsymbol{k}) + T_s\left((V_s)_n - Ci_s(\boldsymbol{k})\right) \tag{20}$$

$$i_s(\boldsymbol{k+1})_n = i_s(\boldsymbol{k}) + T_s\left(C_1\begin{pmatrix} C_2\boldsymbol{\lambda}_s(\boldsymbol{k}) - C_3 i_s(\boldsymbol{k}) \\ +K_r\left((V_s)_n - Ci_s(\boldsymbol{k})\right) \\ -j\omega_r\boldsymbol{\lambda}_s(\boldsymbol{k}) \\ +\frac{j\omega_r i_s(\boldsymbol{k})}{C_1}\end{pmatrix}\right) \tag{21}$$

$$\left(T_{\text{motor}}(k+1)\right)_n = \frac{3}{2}\frac{P}{2}\left(\text{imag}\left(\bar{\boldsymbol{\lambda}}_s(\boldsymbol{k+1})_n \otimes i_s(\boldsymbol{k+1})_n\right)\right) \tag{22}$$

where $n = 0, 1, 2, 3 \ldots..36$.

C. Cost Function Formulation

Cost function deals with number of control objectives. As it involves different objectives, relative balance among them is mandatory. The control action and switching state realization is to minimize the cost function. For IM drive applications, basic cost function is stated by (23). Here, "W" is the weighting factor providing relative importance between torque and flux. However, when the number of objectives is more, weighting factors adjustment for every objective is difficult and has direct impact on optimal VV selection. Therefore, the only adjustable term "W" is influencing the control performance of PTC

$$G_n = \left|T^*_{\text{motor}} - T_{\text{motor}}(k+1)_n\right| + W\left|\lambda^*_s - \left|\boldsymbol{\lambda}_s(\boldsymbol{k+1})_n\right|\right|. \tag{23}$$

Here, the reference stator flux magnitude and motor torque are denoted by λ^*_s and T^*_{motor}, respectively. In literature [21]–[35], various empirical and analytical approaches are proposed to solve the problem of weighing factor selection in a cost function.

IV. Proposed PTC for OEWIM Drive

In conventional PTC, the cost function is formulated with the control objectives of torque and magnitude of stator flux as stated by (23). This demands flux weighting factor ("W") assignment in it. To alleviate the problem of "W" selection for torque and flux control, this paper introduces stator flux space vector control. The proposed PTC block diagram is shown in Fig. 4. The new control objective is formulated with the reference and predicted stator flux space vector as stated by (24). The main idea here is to make the predicted stator flux space vector close to the generated reference stator flux space vector

$$G_n = \left|\boldsymbol{\lambda}^*_s - \boldsymbol{\lambda}_s(\boldsymbol{k+1})_n\right|. \tag{24}$$

The procedure for reference stator flux space vector (λ_s^*) generation is as indicated in Fig. 4. Speed PI controller generates reference motor torque needed to maintain the actual speed of the motor at a given reference speed value. The machine actual stator and rotor flux estimation is done using the mathematical equations as presented in Section II. The reference stator flux magnitude is set to the machine nominal value. Thus, with the information of reference motor torque, reference stator flux magnitude, rotor flux magnitude, and angle, the reference stator flux angle (θ_s^*) are figured out. Therefore, the reference stator flux magnitude and angle (which is in polar form) undergoes polar to complex form conversion, resulting the generated reference stator flux space vector (λ_s^*). The closeness of real part of predicted stator flux space vector with the real part of generated reference stator flux space vector ensures flux control. Similarly, the closeness of imaginary terms of predicted stator flux space vector and generated reference stator flux space vector ensures torque control. Thus, entirely the closeness of predicted stator flux space vector with the generated reference stator flux space vector ensures a combined torque and stator flux magnitude control with a single stator flux space vector control objective. From (24), it is observed that the new cost function is relieved from optimal "*W*" selection.

However, weighting factors cannot be eliminated when additional control objectives are included in cost function as stated by (25). Here "*N*" represents weighting factor for switching frequency control objective. Reduction in the switching frequency of dual inverter is possible when the number of VV state transitions is less. Thus, the control objective for switching frequency reduction is formulated with the previously applied and present applicable VVs. This can be stated by (26) as follows:

$$G_n = |\boldsymbol{\lambda}_s{}^* - \boldsymbol{\lambda}_s(\boldsymbol{k}+\mathbf{1})_n| + N\,|f_{\rm sw}| \tag{25}$$

where

$$f_{\rm sw} = V_s\,(\boldsymbol{k}-\mathbf{1}) - V_s(\boldsymbol{k})_n. \tag{26}$$

Thus, the proposed scheme is extended to alleviate weighting factors' burden completely using the ranking analysis. Fig. 5 depicts the proposed PTC flow graph. The step by step procedure for it is explained as follows.

Step 1: Multiobjective Separation

Stator flux space vector and switching frequency control objectives are considered separately as stated by (27) and (28). Owing to the sample delay problem, two-step ahead prediction is desired. Therefore, control objectives are modified as (29) and (30)

$$(G_1)_n = |\boldsymbol{\lambda}_s{}^* - \boldsymbol{\lambda}_s(\boldsymbol{k}+\mathbf{1})_n| \tag{27}$$

$$(G_2)_n = |V_s\,(\boldsymbol{k}-\mathbf{1}) - V_s(\boldsymbol{k})_n|\,. \tag{28}$$

Control objectives formulated with two-step ahead prediction

$$(G_1)_n = |\boldsymbol{\lambda}_s{}^* - \boldsymbol{\lambda}_s(\boldsymbol{k}+\mathbf{2})_n| \tag{29}$$

$$(G_2)_n = |V_s\,(\boldsymbol{k}) - V_s(\boldsymbol{k}+\mathbf{1})_n| \tag{30}$$

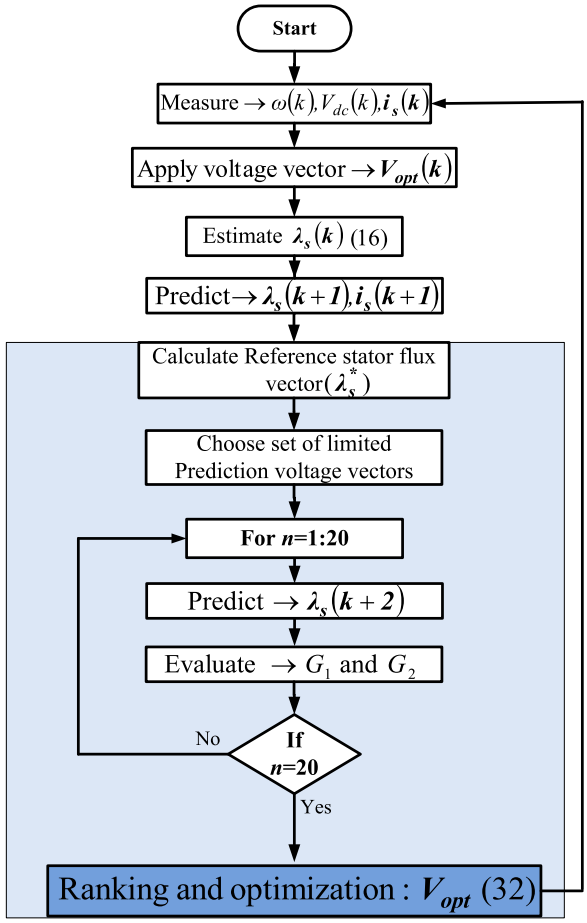

Fig. 5. Proposed PTC flow graph.

where

$$\boldsymbol{\lambda}_s(\boldsymbol{k}+\mathbf{2})_n = \boldsymbol{\lambda}_s\,(\boldsymbol{k}+\mathbf{1}) + T_s\,((V_s\,(\boldsymbol{k}+\mathbf{1}))_n - Ci_s\,(\boldsymbol{k}+\mathbf{1}))\,. \tag{31}$$

Step 2: Assessment and Ranking

The control objectives (G_1 and G_2) are assessed for every available VV. Lower rank of "1" is assigned to the VV for which the control objective value is minimum compared to remaining values. From this value, ranking increases with an increase in the control objective value. As two control objectives are considered, every VV is associated with two ranks (R_1 and R_2).

Step 3: Selection of Optimal Switching State

After assessment and ranking, the averaged rank value is determined for every VV as stated by (32). The VV having minimum averaged rank value is considered as the optimal switching state for the next sample interval.

$$\boldsymbol{V_{opt}} = \mathrm{VV}\left[\min\left(\frac{R_1+R_2}{2}\right)\right]. \tag{32}$$

A. VV Selection

It is known that the dual inverter fed OEWIM offers "37" effective voltage states. Thus, all these states can be considered for the control process. But it demands more computational time. To reduce the computational burden, VVs should be

TABLE II
POSSIBLE SET OF VV PREDICTIONS

Sector number	Set of VVs for $\Delta\lambda_S \geq 0$	Set of VVs for $\Delta\lambda_S < 0$
1	$V_0, V_6, V_1, V_2, V_{16}, V_{17}, V_{18}, V_7, V_8, V_9, V_{10}, V_{33}, V_{34}, V_{35}, V_{36}, V_{19}, V_{20}, V_{21}, V_{22}, V_{23}$	$V_0, V_{24}, V_{25}, V_{26}, V_{27}, V_{28}, V_{29}, V_{30}, V_{31}, V_{32}, V_{10}, V_{11}, V_{12}, V_{13}, V_{14}, V_{15}, V_{16}, V_3, V_4, V_5$
2	$V_0, V_{18}, V_7, V_8, V_9, V_{10}, V_{11}, V_{12}, V_1, V_2, V_3, V_{36}, V_{19}, V_{20}, V_{21}, V_{22}, V_{23}, V_{24}, V_{25}, V_{26}$	$V_0, V_{27}, V_{28}, V_{29}, V_{30}, V_{31}, V_{32}, V_{33}, V_{34}, V_{35}, V_{12}, V_{13}, V_{14}, V_{15}, V_{16}, V_{17}, V_{18}, V_4, V_5, V_6$
3	$V_0, V_8, V_9, V_{10}, V_{11}, V_{12}, V_{13}, V_{14}, V_2, V_3, V_4, V_{21}, V_{22}, V_{23}, V_{24}, V_{25}, V_{26}, V_{27}, V_{28}, V_{29}$	$V_0, V_{30}, V_{31}, V_{32}, V_{33}, V_{34}, V_{35}, V_{36}, V_{19}, V_{20}, V_{14}, V_{15}, V_{16}, V_{17}, V_{18}, V_7, V_8, V_5, V_6, V_1$
4	$V_0, V_{10}, V_{11}, V_{12}, V_{13}, V_{14}, V_{15}, V_{16}, V_3, V_4, V_5, V_{24}, V_{25}, V_{26}, V_{27}, V_{28}, V_{29}, V_{30}, V_{31}, V_{32}$	$V_0, V_{33}, V_{34}, V_{35}, V_{36}, V_{19}, V_{20}, V_{21}, V_{22}, V_{23}, V_{16}, V_{17}, V_{18}, V_7, V_8, V_9, V_{10}, V_6, V_1, V_2$
5	$V_0, V_{12}, V_{13}, V_{14}, V_{15}, V_{16}, V_{17}, V_{18}, V_4, V_5, V_6, V_{27}, V_{28}, V_{29}, V_{30}, V_{31}, V_{32}, V_{33}, V_{34}, V_{35}$	$V_0, V_{36}, V_{19}, V_{20}, V_{21}, V_{22}, V_{23}, V_{24}, V_{25}, V_{26}, V_{18}, V_7, V_8, V_9, V_{10}, V_{11}, V_{12}, V_1, V_2, V_3$
6	$V_0, V_{14}, V_{15}, V_{16}, V_{17}, V_{18}, V_7, V_8, V_5, V_6, V_1, V_{30}, V_{31}, V_{32}, V_{33}, V_{34}, V_{35}, V_{36}, V_{19}, V_{20}$	$V_0, V_{21}, V_{22}, V_{23}, V_{24}, V_{25}, V_{26}, V_{27}, V_{28}, V_{29}, V_8, V_9, V_{10}, V_{11}, V_{12}, V_{13}, V_{14}, V_2, V_3, V_4$

TABLE III
CONTROL OPERATION DURING ONE SAMPLE INTERVAL

VVs($\mathbf{V_s}$)	G_1	G_2	R_1	R_2	$0.5*(R_1+R_2)$
V_0	0.0144	222.222	13	4	8.5000
V_1	0.0088	111.111	6	2	4.0000
V_2	0.0101	192.45	7	3	5.0000
V_6	0.0164	192.45	14	3	8.5000
V_7	**0.0033**	**0**	**1**	**1**	**1.0000**
V_8	0.0045	111.111	3	2	2.5000
V_9	0.0121	222.222	10	4	7.0000
V_{10}	0.0176	293.972	15	5	10.0000
V_{16}	0.024	293.972	19	5	12.0000
V_{17}	0.0184	222.222	16	4	10.0000
V_{18}	0.0108	111.111	9	2	5.5000
V_{19}	0.0086	111.111	5	2	3.5000
V_{20}	0.0043	111.111	2	2	2.0000
V_{21}	0.0065	192.45	4	3	3.5000
V_{22}	0.0141	293.972	12	5	8.5000
V_{23}	0.0197	333.333	17	6	11.5000
V_{33}	0.026	333.333	20	6	13.0000
V_{34}	0.0205	293.972	18	5	11.5000
V_{35}	0.0129	192.45	11	3	7.0000
V_{36}	0.0107	111.111	8	2	5.0000

TABLE IV
OEWIM SPECIFICATIONS

Motor Parameter	Quantity
Stator Resistance (R_s)	4.2 Ω
Rotor Resistance (R_r)	2.67 Ω
Stator Inductance (L_s)	0.54 H
Rotor Inductance (L_r)	0.54 H
Mutual Inductance (L_m)	0.512 H
Poles (P)	4
Inertia (J)	0.031 Kg-m^2
Rated Power (kW)	3.7 kW

limited. This can be possible by knowing the stator flux position and flux error. Considering the instant where stator flux vector location is in Sector 1 and flux error ($\Delta\lambda_s = |\lambda_s^*| - |\lambda_s|$) is $\geq$ 0, the VVs made available to increase flux magnitude are as shown in Fig. 3(b) (Dark side of plane). Similarly for the same location of the stator flux vector, when flux error is < 0, the

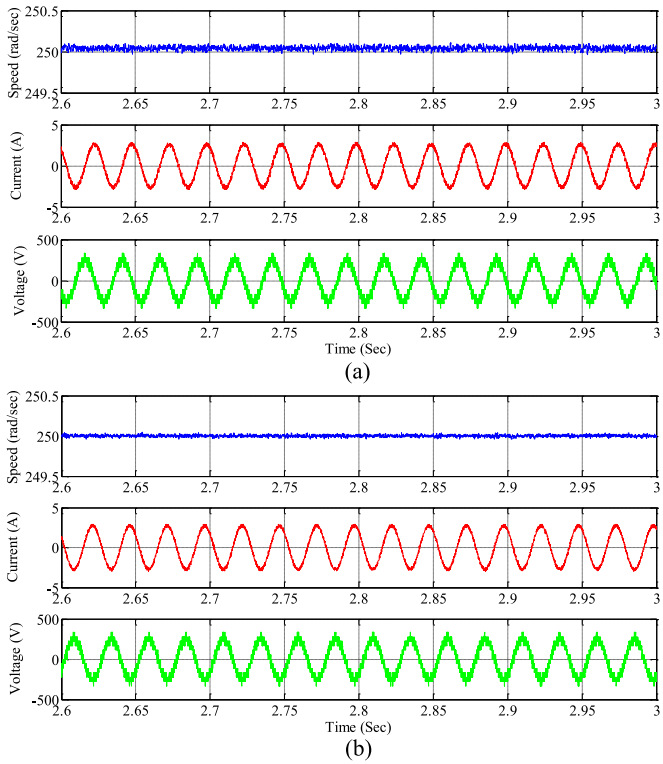

Fig. 6. Simulated steady-state waveforms of voltage and current at speed of 250 rad/s. (a) Conventional PTC. (b) Proposed PTC.

VVs made available to decrease flux magnitude are located at the right side of plane as shown in Fig. 3(b). Thus, with this technique number of prediction, VVs are limited to "'20." It is also possible to find the limited prediction vectors, considering torque error ($T^*_{\text{motor}} - T_{\text{motor}}$). Fig. 3(c) shows limited prediction vectors made available to increase torque when flux vector is located in Sector 1 and torque error ($\Delta\ T$) is $\geq$ 0. But here, prediction VV number increased to "22" compared to the flux error-based technique where it is "20." Therefore, the former technique is used for finding the limited VV predictions.

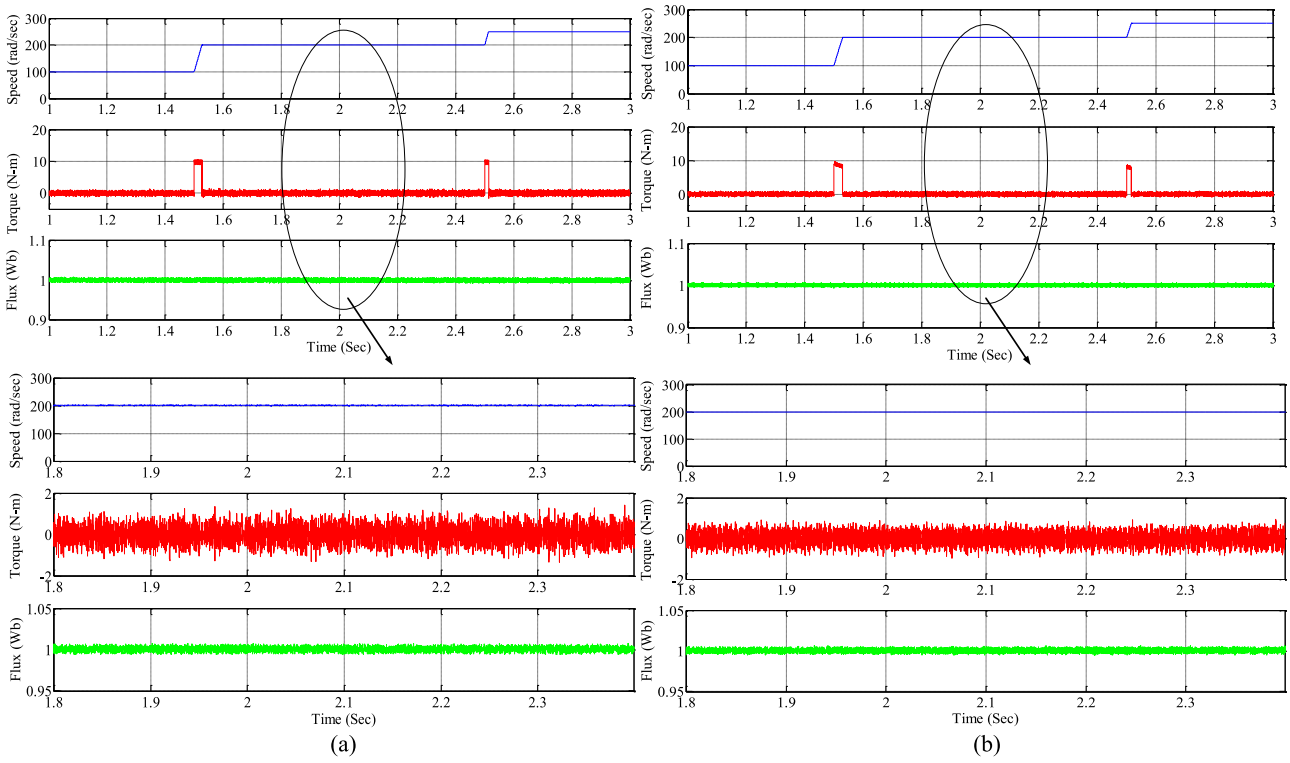

Fig. 7. Speed, torque and flux dynamic characteristics with the step changes in reference speed (100 to 200 rad/s and finally 250 rad/s). (a) Conventional PTC. (b) Proposed PTC.

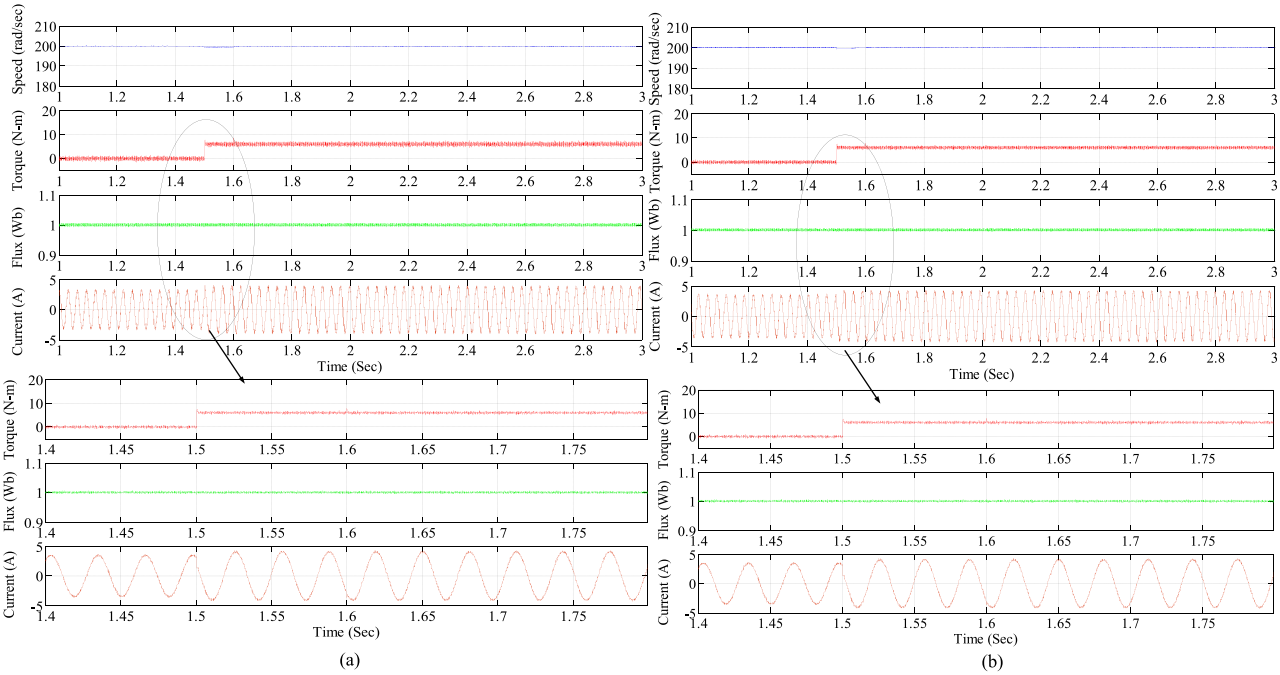

Fig. 8. Simulated dynamic response of motor speed, torque, flux and current at reference speed of 200 rad/s with the step change in load torque. (a) Conventional PTC. (b) Proposed PTC.

Table II represents limited VV predictions in six sectors based on stator flux error condition. Null state (V_0) is always involved with the active vectors (V_1 to V_{36}) for minimizing torque and flux ripples. With this, there are only "20" prediction VVs selected out of "37" in each sample period and made available for a multiobjective ranking analysis. This simplifies control process and computational time is reduced.

The proposed control technique is examined for one sample period. Table III represents control objective values for the available limited VVs in a particular sample period and its

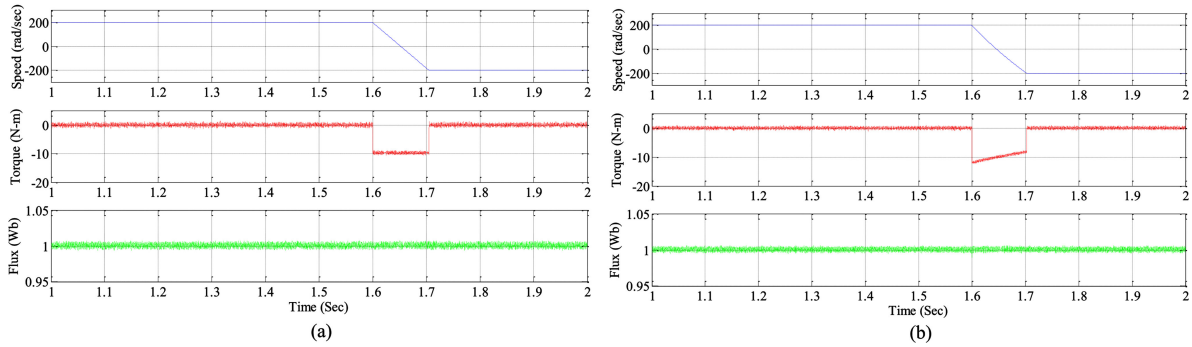

Fig. 9. Simulated forward to reverse motoring dynamic characteristics from +200 to –200 rad/s. (a) Conventional PTC. (b) Proposed PTC.

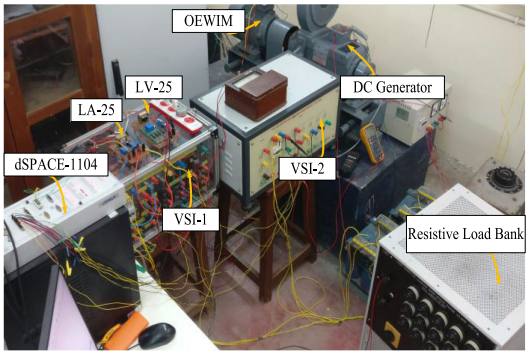

Fig. 10. Experimental test setup.

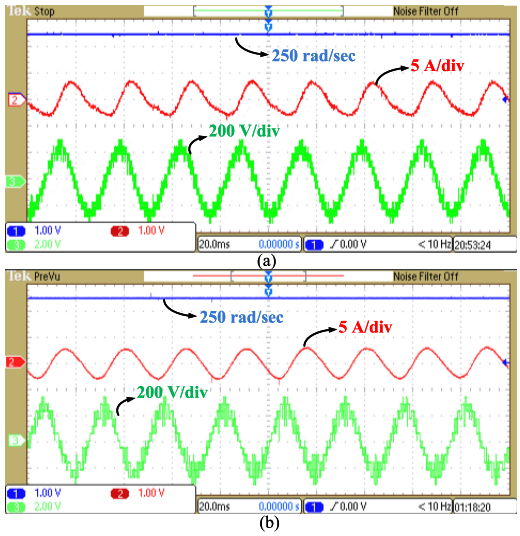

Fig. 11. Steady-state speed, current, and voltage at reference speed of 250 rad/s. (a) Conventional PTC. (b) Proposed PTC.

corresponding rankings. It is observed that the VV V_7 exhibits minimum averaged rank value which is selected as optimal state for dual inverter switching in the next sample interval.

V. Results and Discussion

To check the performance of the proposed PTC of the OEWIM drive, simulation and experimental tests are conducted on existing 3.7-kW, 1440 R/min OEWIM. Its machine

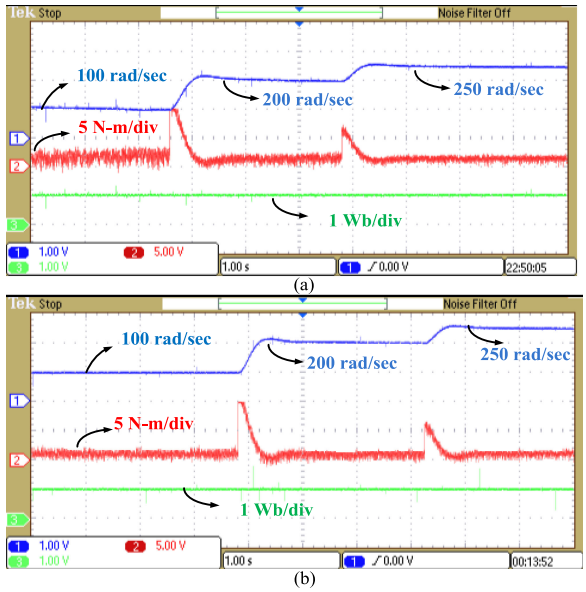

Fig. 12. Dynamic characteristics of the motor speed, torque, and flux at no load. (a) Conventional PTC. (b) Proposed PTC.

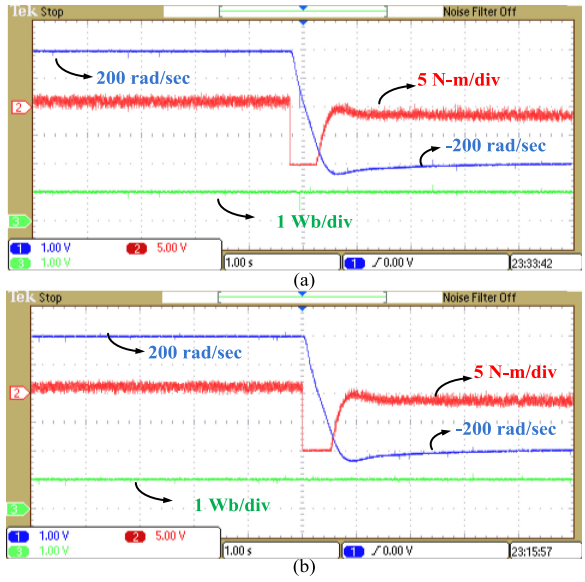

Fig. 13. Speed, torque, and flux dynamic characteristics during forward to reverse motoring operation. (a) Conventional PTC. (b) Proposed PTC.

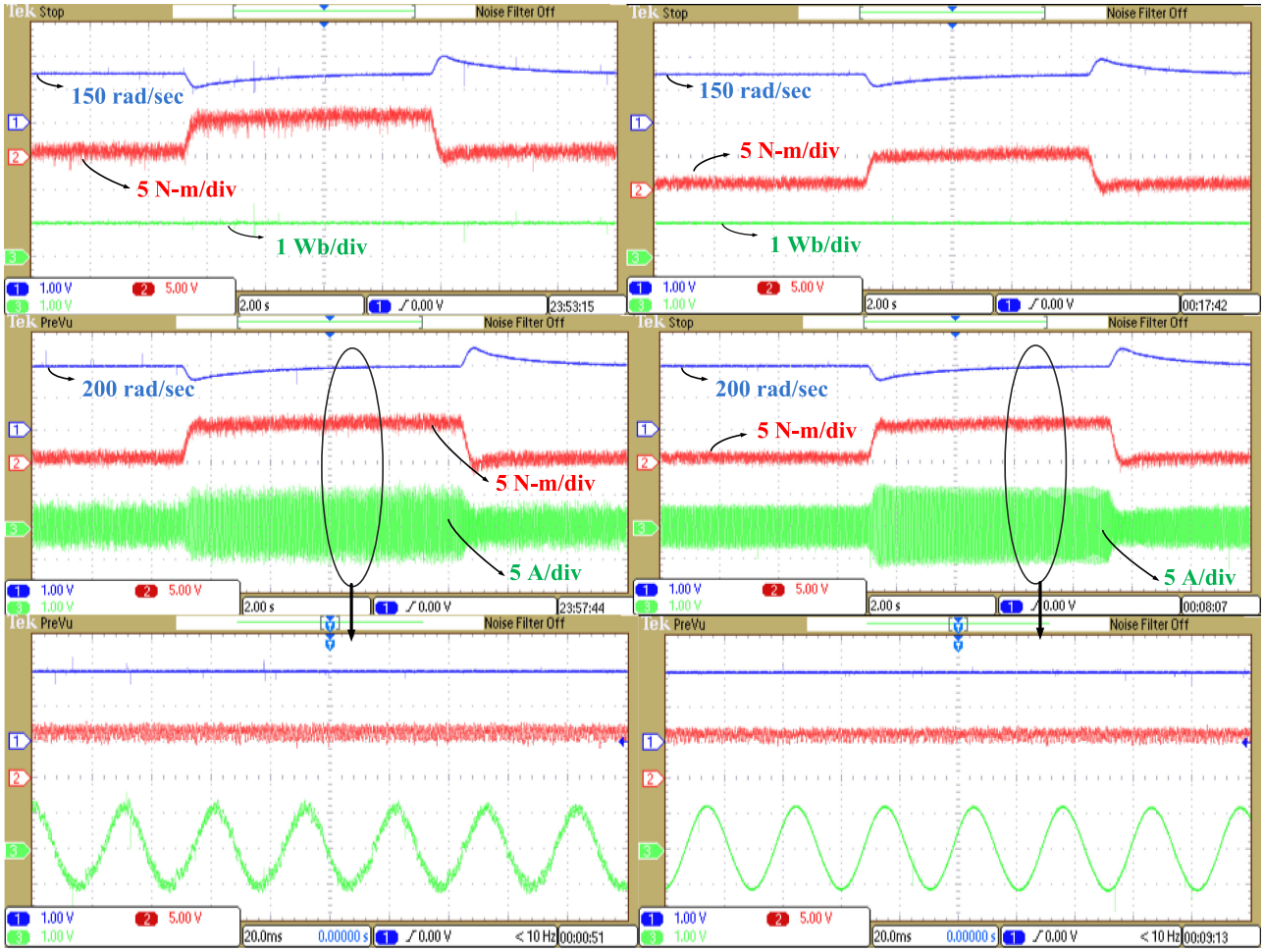

Fig. 14. Motor speed, torque, stator flux, and current dynamic characteristics with step changes in load torque. (a) Conventional PTC. (b) Proposed PTC.

parameters are represented in Table IV. Results are presented in comparison with basic PTC to accentuate its merits. For this, the basic PTC cost function weighting factor is opted conventionally in (23).

A. Simulation Results

The proposed PTC scheme for OEWIM drive as shown in Fig. 4 is simulated in MATLAB software. The dual inverter fed OEWIM is mathematically modeled using (1)–(14). DC-link voltages of the dual inverter are maintained at 333.33 and 166.67 V, i.e., in the ratio of $(2V_{dc}/3)$ and $(V_{dc}/3)$. Here V_{dc} corresponds to combined dc-link voltage which is set to 500 V. The reference stator flux magnitude $(|\lambda_s^*|)$ is set to a nominal value of 1 Wb. The performed simulation results are shown in Figs. 6–9.

Fig. 6 shows the motor speed, phase voltage, and current simulated waveforms at the reference speed of 250 rad/s (electrical). Steady-state characteristics of a machine (speed, motor torque, and stator flux) at the reference speed of 200 rad/s are shown in Fig. 7 in an expanded view. The dynamic performance of a machine is analyzed with step changes in reference speed (100 to 200 rad/s and then 250 rad/s) at no load. Its motor speed, torque, and flux characteristics are shown in Fig. 7. Step changes in load torque are performed from no load to 6 N·m of load. It is observed that motor torque is tracking load torque with low ripple content for the proposed PTC of OEWIM drive. Its dynamic characteristics (speed, torque, current, and flux) at the reference speed of 200 rad/s are shown in Fig. 8.

At no load, the motor reference speed is changed from +200 to –200 rad/s conveying forward to reverse motoring. Its dynamic characteristics are shown in Fig. 9. From these results it is evident that the proposed PTC of OEWIM drive exhibits optimal control response having low-steady-state torque and flux ripples.

B. Hardware Results

The hardware setup of the existing machine as shown in Fig. 10 is used for real-time execution of the proposed PTC of OEWIM drive. The proposed control algorithm is implemented in a discrete platform using dSPACE real-time interfacing (RTI-1104). The sensed dc-link voltages from voltage sensor (LV-25) and stator currents from current sensor (LA-25) are given to

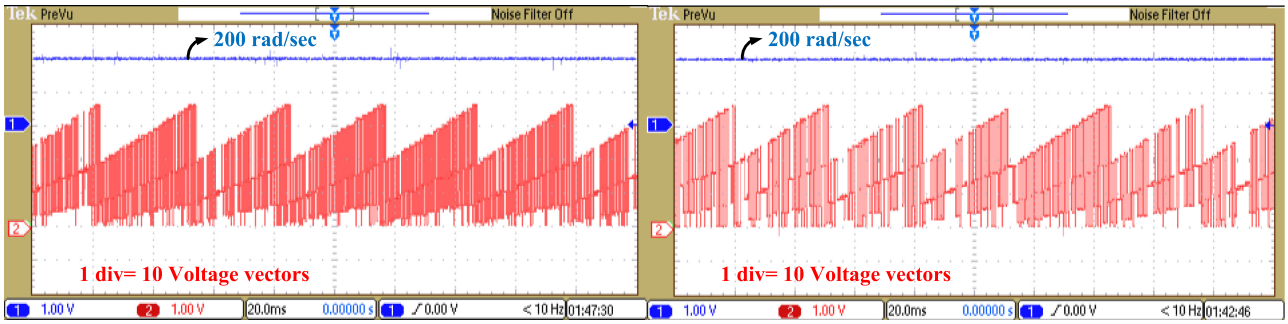

Fig. 15. Switching state transitions at speed of 200 rad/s. (a) Conventional PTC. (b) Proposed PTC.

TABLE V
COMPARATIVE ANALYSIS

Control scheme	Speed	Torque ripple (N-m)	Flux ripple (Wb)	Switching Frequency (Hz)
Conventional PTC	100 rad/s	3.7	0.036	4250
Proposed PTC		2.9	0.03	3860
Conventional PTC	200 rad/s	3.1	0.025	3900
Proposed PTC		2.5	0.018	3610
Conventional PTC	250 rad/s	2.6	0.014	3800
Proposed PTC		1.9	0.012	3500

ADC BNC connectors of dSPACE controller board interfacing. From the motor encoder, speed is measured and interfaced to dSPACE incremental encoder. The controlled switching pulses are acquired at digital I/O pins and processed to interface with inverter switches. The conducted experimental results are shown in Figs. 11–15.

During no load operation, motor speed, phase voltage, and current at the reference speed of 250 rad/s are shown in Fig. 11.

For online step changes in the reference speed, controlDesk software is used. Thus, the dynamic performance of the machine is examined by step changes in reference speeds (100 to 200 rad/s and then 250 rad/s) at no load as shown in Fig. 12. Fig. 13 shows forward to reverse motoring operation at no load, when a step change in the reference speed is given from 200 to –200 rad/s.

For applying load torque, an equivalent resistive load is connected to a dc generator which is coupled to an OEWIM. Thus, by loading the dc generator with a resistive load, step changes in load torque are performed when the motor is operating at a speed of 150 and 200 rad/s. These dynamic experimental results are shown in Fig. 14. Steady-state performance under loaded condition is also shown in Fig. 14.

While in operation, dual inverter switching states are shown in Fig. 15. From this, minimum switching state transitions are observed for the proposed PTC scheme indicating a lower switching frequency. Finally, a comparative table is prepared for flux and torque ripple, and switching frequency achieved in conventional and proposed PTC of OEWIM drive as shown in Table V. These results indicate effectiveness of the proposed PTC over the conventional PTC scheme.

VI. CONCLUSION

In this paper, modified PTC for an OEWIM drive application has been introduced and implemented. This approach eliminates flux weighting factor assignment and provides combined torque and flux control by introducing stator flux space vector based control in a cost function. However, when additional control objective, i.e., switching frequency is involved in a single cost function, the proposed scheme is extended to eliminate weighting factors completely using a multiobjective ranking analysis. To reduce the control algorithm complexity, prediction VVs of OEWIM drive are limited by a stator flux error strategy.

The proposed PTC for OEWIM drive is verified by conducting simulation and experimental tests. These results are examined in comparison with the conventional PTC scheme. It is observed that the OEWIM drive exhibits better torque and flux response for the proposed PTC. Switching frequency of dual inverter also reduced compared to the conventional PTC scheme. Finally, an improvised predictive control is accomplished for the OEWIM drive.

REFERENCES

[1] S. Kouro *et al.*, "Recent advances and industrial applications of multilevel converters," *IEEE Trans. Ind. Electron.*, vol. 57, no. 8, pp. 2553–2580, Aug. 2010.
[2] K. K. Gupta, A. Ranjan, P. Bhatnagar, L. K. Sahu, and S. Jain, "Multilevel inverter topologies with reduced device count: A review," *IEEE Trans. Power Electron.*, vol. 31, no. 1, pp. 135–151, Jan. 2016.
[3] J. Rodriguez, J. S. Lai, and F. Z. Peng, "Multilevel inverters: A survey of topologies, controls, and applications," *IEEE Trans. Ind. Electron.*, vol. 49, no. 4, pp. 724–738, Aug. 2002.
[4] S. Lakhimsetty, N. Surulivel, and V. T. Somasekhar, "Improvised SVPWM strategies for an enhanced performance for a four-level open-end winding induction motor drive," *IEEE Trans. Ind. Electron.*, vol. 64, no. 4, pp. 2750–2759, Apr. 2017.

[5] F. Blaschke, "The principle of field-orientation as applied to the TRANSVECTOR closed-loop control system for rotating-field machines," *Siemens Rev.*, vol. 34, pp. 217–220, 1972.
[6] A. Kawamura and R. Haft, "An analysis of induction motor field oriented or vector control," in *Proc. IEEE Power Electron. Spec. Conf. Rec.*, 1983, pp. 91–101.
[7] S. Sathikumar and J. Vithayathil, "Digital simulation of field-oriented control of induction motor," *IEEE Trans. Ind. Electron.*, vol. IE-31, no. 2, pp. 141–148, May 1984.
[8] Takashi and T. Noguchi, "A new quick-response and high-efficiency control of an induction motor," *IEEE Trans. Ind. Appl.*, vol. 22, no. 5, pp. 820–827, Sep. 1986.
[9] J.-K. Kang and S.-K. Sul, "New direct torque control of induction motor for minimum torque ripple and constant switching frequency," *IEEE Trans. Ind. Appl.*, vol. 35, no. 5, pp. 1076–1082, Sep./Oct. 1999.
[10] K.-B. Lee, J.-H. Song, I. Choy, and J.-Y. Yoo, "Torque ripple reduction in DTC of induction motor driven by three-level inverter with low switching frequency," *IEEE Trans. Power Electron.* vol. 11, no. 2, pp. 255–264, Mar. 2002.
[11] K.-K. Shyu, J.-K. Lin, V.-T. Pham, M.-J. Yang, and T.-W. Wang, "Global minimum torque ripple design for direct torque control of induction motor drives," *IEEE Trans. Ind. Electron.*, vol. 57, no. 9, pp. 3148–3156, Sep. 2010.
[12] R. Ramchand, K. Gopakumar, C. Patel, K. Sivakumar, A. Das, and H. Abu-Rub, "Online computation of hysteresis boundary for constant switching frequency current-error space-vector-based hysteresis controller for VSI fed IM drives," *IEEE Trans. Power Electron.*, vol. 27, no. 3, pp. 1521–1529, Mar. 2012.
[13] M. Morari and J. H. Lee, "Model predictive control: Past, present and future," *Comput. Chem. Eng.*, vol. 23, pp. 667–682, 1999.
[14] J. Maciejowski, *Predictive Control With Constraints*. New York, NY, USA: Prentice-Hall, 2002.
[15] E. Camacho and C. Bordons, *Model Predictive Control*. Berlin, Germany: Springer-Verlag, 2007.
[16] J. Rawlings and D. Mayne, *Model Predictive Control, Theory and Design*. Madison, WI, USA: Nob Hill Publishing, 2009.
[17] A. Linder and R. Kennel, "Model predictive control for electrical drives," in *Proc. IEEE 36th Power Electron. Spec. Conf.*, 2005, pp. 1793–1799.
[18] J. Rodriguez *et al.*, "State of the art of finite control set model predictive control in power electronics," *IEEE Trans. Ind. Informat.*, vol. 9, no. 2, pp. 1003–1016, May 2013.
[19] P. Correa, M. Pacas, and J. Rodriguez, "Predictive torque control for inverter-fed induction machines," *IEEE Trans. Ind. Electron.*, vol. 54, no. 2, pp. 1073–1079, Apr. 2007.
[20] P. Mutschler and E. Flach, "Digital implementation of predictive direct control algorithms for induction motors," in *Proc. IEEE Ind. Appl. Conf.*, 1998, pp. 444–451.
[21] P. Cortes *et al.*, "Guidelines for weighting factors design in model predictive control of power converters and drives," in *Proc. IEEE Int. Conf. Ind. Technol.*, 2009, pp. 1–7.
[22] R. Vargas, J. Rodríguez, U. Ammann, and P. W. Wheeler, "Predictive current control of an induction machine fed by a matrix converter with reactive power control," *IEEE Trans. Ind. Electron.*, vol. 55, no. 12, pp. 4372–4380, Dec. 2008.
[23] J. Rodríguez *et al.*, "High performance control strategies for electrical drives: An experimental assessment," *IEEE Trans. Ind. Electron.*, vol. 59, no. 2, pp. 812–820, Feb. 2012.
[24] R. Vargas, U. Ammann, B. Hudoffsky, J. Rodriguez, and P. Wheeler, "Predictive torque control of an induction machine fed by a matrix converter with reactive input power control," *IEEE Trans. Power Electron.*, vol. 25, no. 6, pp. 1426–1438, Jun. 2010.
[25] H. Miranda, P. Cortes, J. Yuz, and J. Rodriguez, "Predictive torque control of induction machines based on state-space models," *IEEE Trans. Ind. Electron.*, vol. 56, no. 6, pp. 1916–1924, Jun. 2009.
[26] S. A. Davari, D. A. Khaburi, and R. Kennel, "An improved FCS–MPC algorithm for an induction motor with an imposed optimized weighting factor," *IEEE Trans. Power Electron.*, vol. 27, no. 3, pp. 1540–1551, Mar. 2012.
[27] M. Uddin *et al.*, "Model predictive torque ripple reduction with weighting factor optimization fed by an indirect matrix converter," *Electr. Power Compon. Syst.*, vol. 42, no. 10, pp. 1059–1069, 2014.
[28] P. Zanchetta, "Heuristic multi-objective optimization for cost function weights selection in finite states model predictive control," in *Proc. Workshop Predictive Contr. Electr. Drives Power Electron.*, Oct. 2011, pp. 70–75.
[29] C. A. Rojas, J. Rodriguez, F. Villarroel, J. R. Espinoza, C. A. Silva, and M. Trincado, "Predictive torque and flux control without weighting factors," *IEEE Trans. Ind. Electron.*, vol. 60, no. 2, pp. 681–690, Feb. 2013.
[30] V. P. Muddineni, A. K. Bonala, and S. R. Sandepudi, "Enhanced weighting factor selection for predictive torque control of induction motor drive based on VIKOR method," *IET Electr. Power Appl.*, vol. 10, no. 9, pp. 877–888, 2016.
[31] V. P. Muddineni, S. R. Sandepudi, and A. K. Bonala, "Finite control set predictive torque control for induction motor drive with simplified weighting factor selection using TOPSIS method," *IET Electr. Power Appl.*, vol. 11, no. 5, pp. 749–760, 2017.
[32] M. B. Shadmand, R. S. Balog, and H. A. Rub, "Auto-tuning the cost function weight factors in a model predictive controller for a matrix converter VAR compensator," in *Proc. IEEE Energy Convers. Congr. Expo.*, Montreal, QC, Canada, 2015, pp. 3807–3814.
[33] C. A. Rojas, S. Kouro, M. Perez, and F. Villarroel, "Multiobjective Fuzzy Predictive Torque Control of an induction machine fed by a 3L-NPC inverter," in *Proc. IEEE Int. Symp. Predictive Contr. Electr. Drives Power Electron.*, Valparaiso, IN, USA, 2015, pp. 21–26.
[34] B. Zhu, K. Rajashekara, and H. Kubo, "Predictive torque control with zero-sequence current suppression for open-end winding induction machine," in *Proc. IEEE Ind. Appl. Soc. Annu. Meet.*, Addison, TX, USA, 2015, pp. 1–7.
[35] K. V. P. Kumar and T. V. Kumar, "Predictive torque control of open-end winding induction motor drive fed with multi-level inversion using two two-level inverters," *IET Electric Power Appl.*, vol. 12, no. 1, pp. 54–62, 2018, DOI: 10.1049/iet-epa.2017.0209.
[36] J. Rodriguez and P. Cortes, "Predictive control of induction machines," in *Predictive Control of Power Converters and Electrical Drives*. New York, NY, USA: Wiley-IEEE Press, 2012, pp. 115–132.

Ravi Eswar Kodumur Meesala was born in Kurnool, India, in 1993. He received the B.Tech. degree from Jawaharlal Nehru Technological University, Ananthapur, India, in 2014, and the M.Tech. degree from the Vellore Institute of Technology, Vellore, India, in 2016. He is currently working toward the Ph.D. degree with the Department of Electrical Engineering, National Institute of Technology, Warangal, India.

His current research interests include electric motor drive control, power electronics, and power converter circuits.

Venkata Praveen Kumar Kunisetti was born in Guntur, India, in 1990. He received the B.Tech. and M.Tech. degrees from Jawaharlal Nehru Technological University, Kakinada, India, in 2011 and 2014, respectively. He is currently working toward the Ph.D. degree with the Department of Electrical Engineering, National Institute of Technology, Warangal, India.

His current research interests include electric motor drive control, power electronics, and power converter circuits.

Vinay Kumar Thippiripati was born in Kadapa, India, in 1984. He received the B.Tech. and M.Tech. degrees from Jawaharlal Nehru Technological University, Hyderabad, India, in 2005 and 2008, respectively. He received the Ph.D. degree from the National Institute of Technology, Warangal, India, in 2015.

In 2013, he joined in National Institute of Technology, Warangal, India, as an Assistant Professor. His research interests include power electronics and drives, direct torque control, predictive torque control, open-end winding induction motor drives, multilevel inverters, hybrid electric vehicles, and renewable energy interfacing.